Applied Catalysis B: Environmental 246 (2019) 100–110

Contents lists available at ScienceDirect

Applied Catalysis B: Environmental

journal homepage: www.elsevier.com/locate/apcatb

Direct transformation of terminal alkenes with H_2O into primary alcohols over metal oxide-supported Pd catalysts

Zhenzhong Zhang[a], Tetsuya Mamba[a], Eiji Yamamoto[a], Haruno Murayama[a], Tamao Ishida[b,c,**], Tetsuo Honma[d], Tadahiro Fujitani[e], Makoto Tokunaga[a,*]

[a] Department of Chemistry, Graduate School of Science, Kyushu University, 744 Motooka, Nishi-ku, Fukuoka, 819-0395, Japan
[b] Research Center for Gold Chemistry, Graduate School of Urban Environmental Sciences, Tokyo Metropolitan University, 1-1 Minami-Osawa, Hachioji, Tokyo, 192-0397, Japan
[c] Department of Applied Chemistry for Environment, Graduate School of Urban Environmental Sciences, Tokyo Metropolitan University, 1-1 Minami-Osawa, Hachioji, Tokyo, 192-0397, Japan
[d] Japan Synchrotron Radiation Research Institute (JASRI), SPring-8, Sayo, Hyogo, 679-8198, Japan
[e] National Institute of Advanced Industrial Science and Technology (AIST), 16-1 Onogawa, Tsukuba, Ibaraki, 305-8569, Japan

ARTICLE INFO

Keywords:
Primary alcohols
Palladium catalysts
Terminal alkenes
Anti-Markovnikov
Allylic alcohols

ABSTRACT

The *anti*-Markovnikov addition of H_2O to alkenes to directly bring in primary alcohols has been considered one of the "10 challenges in catalysis" in the 1990s, but the challenging issue has still remained unsolved over the past few decades, particularly in terms of developing an atom-efficient synthetic strategy. In this context, we introduce a novel access for the transformation of terminal alkenes with H_2O into the corresponding primary alcohols over metal oxide-supported Pd catalysts, employing O_2 as the sole oxidant. Direct and efficient synthesis of cinnamyl alcohol from allylbenzene and H_2O was initially achieved as a fine chemical example over Pd$(NO_3)_2$/CeO_2-ZrO_2, and the target saturated alcohol (3-phenylpropan-1-ol) was obtained as the *anti*-Markovnikov selective product from a "*one-pot*" process using H_2 as the reductant. The Pd$(NO_3)_2$/CeO_2-ZrO_2 was characterized by HAADF-STEM, XRD and X-ray absorption fine structure (XAFS) analyses, indicating that the molecular Pd$(NO_3)_2$ is probably deposited as it is on the support, which likely plays an important role to promote this reaction. In the second part, Pd$(NO_3)_2$/CeO_2-ZrO_2 and other supported Pd catalysts were applied for the transformation of 1,3-butadiene into 2-butene-1,4-diol in a batch reactor. Besides, butane-1,4-diol, which is an important industrial material, was efficiently produced by the simple hydrogenation of 2-butene-1,4-diol in a "*one-pot*" manner. Significantly, the development of the reaction catalyzed by supported Pd in a gas flow reactor bestows great potential to further industrial applications. Additionally, the adsorption structure of 1,3-butadiene on Pd(111) was confirmed as the *s-trans* form by infrared reflection absorption spectroscopy (IRAS) measurements. The change in the electronic states of surface Pd atoms upon oxygen adsorption was observed by X-ray photoelectron spectroscopy (XPS).

1. Introduction

Development of the atom-efficient synthetic strategies has long since been expected to achieve the significant goal of green chemistry on minimizing the production waste and reducing the depletion of fossil fuel resources [1–3]. In particular, utilization of environmentally benign reactants such as O_2 (or air), H_2, and H_2O to facilitate the industrial applications of synthetic reactions has attracted much attention [4–9]. Primary alcohols are fundamental building-blocks for producing a broad range of chemical commodities, such as detergents and plasticizers [10,11]. Direct installation of a hydroxyl group (−OH) from H_2O into a terminal alkene is regarded as an ideal approach for the synthesis of primary alcohols with a great commercial value [12,13]. However, the ordinary acid-catalyzed hydration of alkenes affords only secondary alcohols in accordance with Markovnikov's rule. Moreover, the reaction suffers from low yield because the equilibrium of the hydration lies on the side of elimination [14]. As a consequence, a two-step process consisting of the hydroformylation of terminal alkenes into

* Corresponding author.
** Corresponding author at: Research Center for Gold Chemistry, Graduate School of Urban Environmental Sciences, Tokyo Metropolitan University, 1-1 Minami-Osawa, Hachioji, Tokyo, 192-0397, Japan.
E-mail addresses: tamao@tmu.ac.jp (T. Ishida), mtok@chem.kyushu-univ.jp (M. Tokunaga).

https://doi.org/10.1016/j.apcatb.2019.01.031
Received 21 August 2018; Received in revised form 9 January 2019; Accepted 12 January 2019
Available online 15 January 2019
0926-3373/

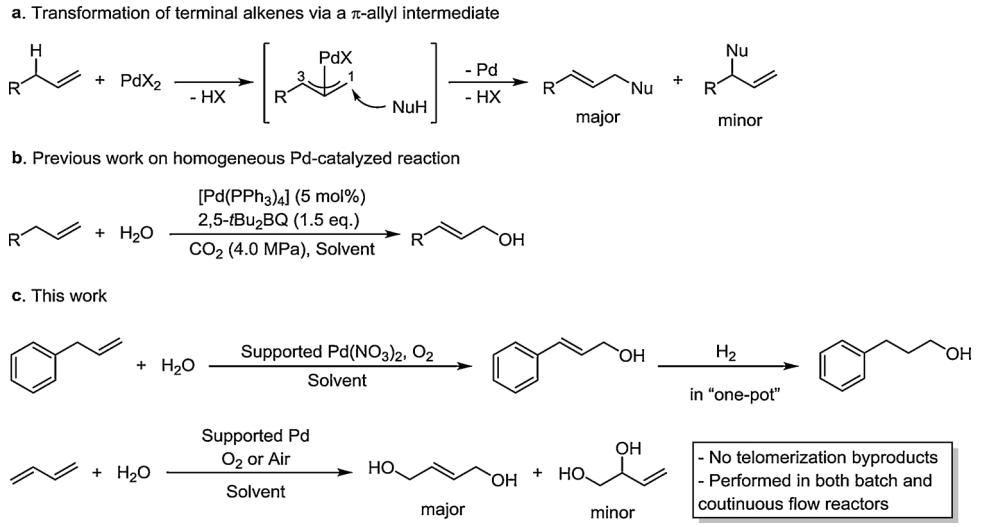

Scheme 1. Allylic oxidation of terminal alkenes for synthesizing primary alcohols and derivatives.

aldehydes followed by a hydrogenation step is mostly adopted in the current chemical industry [15]. Several formal *anti*-Markovnikov hydrations with multiple steps have been exploited, such as a hydroboration-oxidation sequence [14] and a method combining terminal-selective Wacker oxidation followed by reduction [16]. However, multicomponent metal complexes or stoichiometric reagents and oxidants are commonly required, resulting in low atom efficiency, and their industrial applications also remain out of reach.

On the other hand, the catalytic transformation of terminal alkenes into a π-allyl intermediate followed by a nucleophilic attack at the less-hindered terminal position is an attractive way to build linear products (Scheme 1a). Over the past decades, a number of *anti*-Markovnikov selective processes have been developed, including acetoxylation [17–19], alkylation [20], amination [21], amidation [22], etherification [23], esterification [24], carboxylation [25], and trifluoromethoxylation [26]. However, the majority of these reactions proceed in the presence of strong nucleophiles, and H_2O has seldom been used [27]. For example, Showa Denko commercialized an industrial process for the production of allyl alcohol from propene over a supported Pd catalyst, and C—H acetoxylation has been applied as an initial step [17]. Mitsubishi Chemical developed a supported Pd-Te catalyst to convert 1,3-butadiene into butane-1,4-diol in the 1970s. However, the synthetic route to deliver the alcohol products includes three steps: allylic acetoxylation, alkene reduction and ester hydrolysis [18,19,28]. For several notable fine chemical examples, Stahl et al. and Kaneda et al. individually reported similar strategies to achieve the transformation of terminal alkenes into primary alcohols starting from allylic C—H acetoxylation [29,30]. Manyik et al. reported an interesting reaction of 1,3-butadiene with H_2O, but the real nucleophile is carbonate, which is generated from H_2O and pressurized CO_2. Additionally, the telomerization of 1,3-butadiene is unavoidable [31]. Our group previously reported a homogeneous Pd-catalyzed reaction to yield primary alcohols from terminal alkenes, but pressurized CO_2 was necessary. In addition, stoichiometric benzoquinone derivatives have to be employed as the oxidant (Scheme 1b) [32].

With several advantages in terms of separation and recycling, supported metal catalysts have been intensively investigated in both fine and bulk chemical synthesis [33–37]. Very recently, we developed several heterogeneously catalyzed oxidation reactions, such as C—H bond functionalization [38,39], allylic acetoxylation [40], and Wacker oxidation [41]. Herein, we first disclose a practical access for the direct conversion of terminal alkenes with H_2O into primary alcohols over a metal oxide-supported Pd catalyst using O_2 as the sole oxidant. The target saturated alcohols can be acquired by a subsequent simple hydrogenation in a "one-pot" sequence. Most of all, the catalyst allows the production of 2-butene-1,4-diol from 1,3-butadiene without the formation of telomerization byproducts in the absence of stoichiometric organic or inorganic additives (Scheme 1c).

2. Experimental

2.1. Material

Palladium nitrate ($Pd(NO_3)_2$) aqueous solution (200 g_{-Pd}/L) and palladium chloride ($PdCl_2$) were purchased from Tanaka Kikinzoku KK. Palladium acetate ($Pd(OAc)_2$) was purchased from Wako Pure Chemical Industries. Al_2O_3 with a specific surface area of 179 m^2/g was purchased from Mizusawa Chemicals. TiO_2 (anatase) with a specific surface area of 312 m^2/g (ST-111) was supplied from Titan Kogyo. CeO_2 with a specific surface area of 58 m^2/g was obtained from Kojundo Chemical Laboratory. ZrO_2 (RC-100) and CeO_2-ZrO_2 (containing 40% CeO_2) with specific surface areas of 91 m^2/g and 54 m^2/g, respectively, were Japan Reference Catalysts which were supplied by the Catalysis Society of Japan. MgO (JRC-MGO-3) with a specific surface area of 14 m^2/g was supplied by Ube Material Industries. ZnO was purchased from Wako Pure Chemical Industries. Palladium hydroxide on activated carbon (20 wt% $Pd(OH)_2$/C) was purchased from Sigma-Aldrich. All commercial starting materials and reagents were used as received.

2.2. Catalyst preparation

Pd/ZrO_2 and PdO/CeO_2-ZrO_2 catalysts were prepared by the impregnation (IMP) method. The palladium loading was adjusted to 5 wt %. $Pd(NO_3)_2$ aqueous solution (570 μL) was diluted in a small amount of water. ZrO_2 or CeO_2-ZrO_2 (1.0 g) was added to the aqueous solution and stirred at RT for 30 min. After impregnation, H_2O was removed by freeze-drying. The obtained catalysts were calcined at 550 °C for 4 h to obtain PdO/ZrO_2 and PdO/CeO_2-ZrO_2. Then, PdO/ZrO_2 was reduced in a flow of pure H_2 (20 mL/min) at 200 °C for 2 h to obtain Pd/ZrO_2 [41].

Metal oxide supported $Pd(OH)_2$ catalysts were prepared by the deposition-precipitation (DP) method. The palladium loading was adjusted to 5 wt%. $Pd(NO_3)_2$ aqueous solution (570 μL) was dissolved in 400 mL distilled water. The solution was warmed to 70 °C, and the pH of the solution was adjusted to 8 by adding 1.0 M NaOH aqueous solution. Then, the metal oxide support (1.0 g) was added to the solution, and the suspension was stirred at 70 °C for 1 h. The solid was filtered, washed with water, and then dried in air at 70 °C overnight [42].

$Pd(NO_3)_2/CeO_2$-ZrO_2 catalysts were prepared by a modified

impregnation (IMP) method. The palladium loading was adjusted to 5 wt%. $Pd(NO_3)_2$ aqueous solution (570 μL) was dissolved in 100 mL of water. CeO_2-ZrO_2 (1.0 g) was added to the aqueous solution and stirred at RT for 2 h. After impregnation, H_2O was removed by freeze drying to obtain $Pd(NO_3)_2/CeO_2$-ZrO_2.

The catalyst preparation methods in this work are summarized in Scheme S1, Supplementary Information.

2.3. Characterization

High angle annular dark-field scanning transmission electron microscopy (HAADF-STEM) observations were performed using a JEOL JEM-ARM200F. The palladium amounts in the catalysts were analyzed by microwave plasma-atomic emission spectrometry (MP-AES) using an Agilent 4100 MP-AES. Powder X-ray diffraction (XRD) patterns were obtained on a Rigaku MiniFlex600 with a high-intensity CuK_α radiation source (λ = 0.15418 nm). X-ray absorption fine structure (XAFS) measurements were performed at the BL14B2 beamline of SPring-8 (Hyogo, Japan) [43,44]. The XAFS samples were ground with boron nitride in an agate mortar and compacted into pellets. Pd K-edge (24.3 keV) XAFS spectra were measured using a Si (311) double–crystal monochromator in transmission mode. The spectral analysis was performed using the XAFS analysis software Athena and REX2000 (Rigaku Co.) [45]. The experiments of temperature-programmed desorption of CO_2 (CO_2-TPD) and temperature-programmed oxidation (TPO) were individually performed using a BELCAT, MicrotracBEL, equipped with thermal conductivity detector (TCD) and a mass spectrometry (BELMass). For CO_2-TPD, the samples (62 mg) were pretreated at 100 °C in Ar (40 mL/min) for 10 min, and then He (40 mL/min) for 60 min. After pretreatment, the temperature was decreased to 30 °C, and 4.5–5.5% CO_2 in He (40 mL/min) was introduced into the cell at 30 °C for 60 min. The samples were tested from RT to 800 °C in a flow of He (40 mL/min) at a ramping rate of 10 °C/min. The experiment of TPO was carried out with 5% O_2 in He (40 mL/min) from RT to 700 °C at a ramping rate of 5 °C/min.

Conversions and product yields for the transformation of 3-phenyl-1-propene (allylbenzene) into 3-phenyl-2-propen-1-ol (cinnamyl alcohol), 3-phenyl-2-propenal (cinnamaldehyde), phenyl-2-propanone (phenyl acetone) and 3-phenylpropan-1-ol were analyzed by gas chromatography (GC) using an Agilent, GC 6850 Series II equipped with a flame ionization detector (FID) and a J&W HP-1 column (0.25 μm thickness, 0.32 mm I.D., 30 m) using tridecane as an internal standard. Conversions and product yields for the transformation of buta-1,3-diene (1,3-butadiene) into 2-butene-1,4-diol were analyzed by GC using an Agilent GC 6850 Series II equipped with FID and a J&W HP-INNOWAX column (0.25 μm thickness, 0.32 mm I.D., 30 m) using tridecane as an internal standard. GC mass spectrometry (GC–MS) analysis was performed with a Thermo Fisher Scientific Polaris Q equipped with a J&W HP-1 column (0.25 μm thickness, 0.25 mm I.D., 30 m). ^1H and ^{13}C NMR spectra were recorded on a JEOL JNM-ECS400 spectrometer at 400 and 100 MHz, respectively. ^1H assignment abbreviations are as follows: singlet (s), doublet (d), triplet (t), quintet (quin), double of doublet (dd), double of triplet (dt), and multiplet (m). Analytical thin-layer chromatography (TLC) was performed with Merck, TLC silica gel 60 F254 plates. Column chromatography was performed on silica gel (Kanto Chemicals, Silica gel 60 N, spherical, neutral, particle size 40–100 μm).

2.4. General procedures for the transformation of alkenes into primary alcohol in an autoclave

A glass tube placed in an autoclave was charged with Pd catalyst (Pd 2.5 mol%), allylbenzene (1 mmol), distilled water (10 mmol), DMSO (2 mL), and a magnetic stirring bar. The autoclave was purged and filled with O_2 until the pressure reached 0.5 MPa and then stirred at 80 °C for 48 h. After the reaction, the mixture was filtered, and the filtrate was analyzed by GC using tridecane as an internal standard.

2.5. General procedures for the transformation of 1,3-butadiene into 2-butene-1,4-diol in an autoclave

A glass tube placed in an autoclave was charged with distilled water (5 mmol), Pd catalyst (Pd 0.5 mol%), DMSO (2 mL), and a magnetic stirring bar. The autoclave was placed in a liquid nitrogen bath to decrease the temperature to below 0 °C, and 1,3-butadiene (25–60 mmol) was added to the autoclave. The autoclave was purged and filled with O_2 until the pressure reached 1.0 MPa, and then stirred at 60 °C for 48 h. After the reaction, the mixture was filtered, and the filtrate was analyzed by GC using tridecane as an internal standard.

2.6. General procedures for the transformation of 1,3-butadiene into 2-butene-1,4-diol in a gas flow reactor

The Pd catalyst (100 mg) was placed into a fixed bed reactor and clamped by glass wool. The inlet and outlet were closed, and the reactor was pressurized by air to 0.1 or 3.0 MPa monitored by a pressure gage. After the vaporizer was heated to 130 °C and the reactor was heated to 60 or 80 °C, 0.78% 1,3-butadiene in N_2 combined with H_2O (0.5 mL/min) was simultaneously injected into the vaporizer. The reaction mixture was collected every 2 h and analyzed by GC.

3. Results and discussion

3.1. Optimization of reaction conditions

The synthesis of cinnamyl alcohol (**2a**) from allylbenzene (**1**) and H_2O was investigated as a model reaction under aerobic conditions over Pd/ZrO_2 which is an efficient catalyst to promote the Wacker oxidation of terminal alkenes with H_2O [41]. DMSO was used as the solvent because it has shown positive effects in both homogeneous [46] and heterogeneous Pd-catalyzed oxidation reactions [47]. Although **2a** was not obtained, cinnamaldehyde (**2b**), as an *anti*-Markovnikov selective product, and phenylacetone (**2c**), as a Wacker oxidation product, were detected (Table 1, entry 1). According to our previous work that supported $Pd(OH)_2$ as a practical catalyst for C—H bond functionalization [38], ZrO_2-supported $Pd(OH)_2$ was employed for the reaction and conferred **2a** in 37% yield (Table 1, entry 2). Inspired by this finding, various metal oxide-supported $Pd(OH)_2$ catalysts were evaluated by the turnover numbers (TONs) based on the amount of Pd added and the *anti*-Markovnikov selectivity of the products under the same reaction conditions. Relatively acidic metal oxide-supported Pd catalysts, such as $Pd(OH)_2/Al_2O_3$ and $Pd(OH)_2/TiO_2$, gave poor material balance (Table 1, entries 3 and 4). In particular, $Pd(OH)_2/Al_2O_3$ could promote the reaction with a high TON, while the selectivity for **2a** was poor due to the formation of a large amount of **2c** and other polymerized compounds. When MgO and ZnO were selected as the basic supports for Pd $(OH)_2$, low TONs and product yields were obtained, although the formation of **2c** could be efficiently inhibited (Table 1, entries 5 and 6). Among these catalysts, $Pd(OH)_2/CeO_2$ displayed good activity and provided the *anti*-Markovnikov selective products in better yield than the other catalysts (Table 1, entry 7). Therefore, the acid-base property of metal oxides notably influences the reactivity and product selectivity, but other factors cannot be neglected. Direct addition of a base or an acid to adjust the acid-base property of the reaction was examined. However, neither inorganic nor organic base improved the yield, and the conversion of **1** was markedly decreased when a base was introduced (see, Supplementary Information, Table S1, entries 1–4). Benzoquinones, which are known as useful oxidants to promote the functionalization of C—H bonds over homogeneous Pd catalysts, were effective in improving the conversion and selectivity to primary alcohol **2a** (Table 1, entries 8 and 9). This result suggested that the oxidant played an important role in facilitating the reaction. Thus, the reaction

Table 1
Reaction conditions for transformation of allylbenzene and its derivatives into primary alcohols.[a]

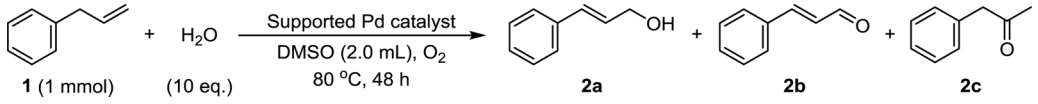

1 (1 mmol) (10 eq.) **2a** **2b** **2c**

Entry	Catalyst	O_2 (MPa)	Conv. (%)[b]	Yield (%)[b]			TONs	*anti*-Markovnikov selectivity (%)[c]
				2a	**2b**	**2c**		
1	5 wt% Pd/ZrO_2	0.5	92	0	21	14	37	23
2	5 wt% $Pd(OH)_2/ZrO_2$	0.5	97	37	16	9	39	55
3	5 wt% $Pd(OH)_2/Al_2O_3$[d]	0.5	97	17	10	30	65	28
4	5 wt% $Pd(OH)_2/TiO_2$	0.5	59	7	4	8	24	19
5	5 wt% $Pd(OH)_2/MgO$	0.5	8	0	2	0	3	25
6	5 wt% $Pd(OH)_2/ZnO$	0.5	65	17	15	0	26	49
7	5 wt% $Pd(OH)_2/CeO_2$	0.5	81	46	13	10	32	73
8[e]	5 wt% $Pd(OH)_2/CeO_2$	0.5	> 99	67	10	20	–	78
9[f]	5 wt% $Pd(OH)_2/CeO_2$	0.5	> 99	74	12	13	–	87
10	5 wt% $Pd(OH)_2/CeO_2$	2.0	92	60	14	11	–	80
11	5 wt% $Pd(OH)_2/CeO_2$-ZrO_2	0.5	82	59	11	5	33	85
12	5 wt% PdO/CeO_2-ZrO_2	0.5	12	0	0	0	5	0
13	5 wt% $Pd(NO_3)_2/CeO_2$-ZrO_2	0.5	98	77	12	9	39	91
14	$Pd(NO_3)_2$	0.5	50	0	0	17	20	0
15	CeO_2-ZrO_2	0.5	3	0	0	0	–	0
16	$Pd(NO_3)_2$ + CeO_2-ZrO_2	0.5	58	0	0	4	23	0
17	5 wt% $Pd(NO_3)_2/CeO_2$-ZrO_2[g]	1.0	> 99	80	11	8	–	92

DMSO = dimethyl sulfoxide.
[a] Reaction conditions: **1** (1 mmol), catalyst (Pd 2.5 mol%), DMSO (2 mL), H_2O (10 equiv.), O_2 (0.5–2.0 MPa), 80 °C, 48 h.
[b] GC analysis using tridecane as an internal standard.
[c] Calculated from the percentage of **2a** and **2b** in all the products.
[d] 5 wt% $Pd(OH)_2/Al_2O_3$ (Pd 1.5 mol%) was used.
[e] Benzoquinone (20 mol%) was added.
[f] 2,5-Di-*tert*-butyl-1,4-benzoquinone (20 mol%) was added.
[g] 5 wt% $Pd(NO_3)_2/CeO_2$-ZrO_2 (Pd 5.0 mol%) was used.

was performed by increasing the pressure of oxygen to 2.0 MPa, and 92% of **1** was converted with better primary alcohol selectivity (Table 1, entry 10). Interestingly, when CeO_2-ZrO_2 mixed oxide (40% CeO_2 component) was used as the support, the reaction proceeded smoothly to afford **2a** in 59% yield with total 85% of *anti*-Markovnikov selective products (Table 1, entry 11).

We compared the catalytic activity of supported $Pd(OH)_2$, PdO, and $Pd(NO_3)_2$ on the same support. Specifically, the $Pd(NO_3)_2$ precursor was simply adsorbed on CeO_2-ZrO_2 to form $Pd(NO_3)_2/CeO_2$-ZrO_2, and PdO/CeO_2-ZrO_2 was prepared by calcined at 300 °C. These catalysts were tested under the same reaction conditions as entry 11. We confirmed that the TON was sharply decreased after calcination treatment (Table 1, entry 12). However, $Pd(NO_3)_2/CeO_2$-ZrO_2 surprisingly showed better activity than $Pd(OH)_2/CeO_2$-ZrO_2 (Table 1, entry 13). Product **2a** was obtained in 77% yield over $Pd(NO_3)_2/CeO_2$-ZrO_2, and the total *anti*-Markovnikov selectivity reached 91%. The TON was calculated to be 39, suggesting that CeO_2-ZrO_2-supported $Pd(NO_3)_2$ is the suitable catalyst for converting allylbenzene. Very recently, Jiang and co-workers developed a homogeneous process for the synthesis of **2a** from **1** catalyzed by $PdCl_2$ [27], but the TON of their catalyst was only 9, and the turnover frequency of their catalyst was also lower than $Pd(NO_3)_2/CeO_2$-ZrO_2 (0.38 h^{-1} vs. 0.81 h^{-1}). Most importantly, a large amount of HCl, which not only causes reactor corrosion but also lowers product selectivity by generating chlorinated byproducts, was required in their process. The use of $Pd(NO_3)_2$ resulted in no desired products, forming Pd black precipitates in the reaction mixture (Table 1, entry 14). In addition, CeO_2-ZrO_2 was also examined for this reaction, but no target product was formed (Table 1, entry 15). These results demonstrate that the catalytic activity of $Pd(NO_3)_2$ was significantly improved when supported on CeO_2-ZrO_2. When $Pd(NO_3)_2$ combined with CeO_2-ZrO_2 was used, only a 4% yield of **2c** was obtained (Table 1, entry 16). Furthermore, the full conversion of **1** was achieved by adjusting the pressure of O_2 and the amount of Pd; 92% of the *anti*-Markovnikov selective products were obtained (Table 1, entry 17). A brief exploration of substrate generality suggested that the introduction of substituents on the aromatic ring of **1** decreased reactivity, especially when bulky or electron-withdrawing groups were placed. Further optimization is required for each substrate.

Notably, we confirmed that a formal *anti*-Markovnikov hydration could be attained via a tandem O_2-H_2 redox step over the 5 wt% Pd $(NO_3)_2/CeO_2$-ZrO_2 catalyst. Allylbenzene was also used as the substrate under the optimized reaction conditions (Table 1, entry 13). After O_2 was released, no additional catalyst was required for the hydrogenation step; the reactor was sealed with 0.5 MPa of H_2 followed by heating at 60 °C for 3 h, and the reaction gave 3-phenylpropan-1-ol in 89% total yield from cinnamyl alcohol and cinnamaldehyde. Phenylacetone could not be reduced in the second step (Scheme 2).

3.2. Characterization of the catalysts

The generation of Pd particles was not observed by HAADF-STEM studies for CeO_2-ZrO_2-supported Pd catalysts, because Pd and CeO_2 or CeO_2-ZrO_2 could not be distinguished due to the high atomic weight of Ce (see, Supplementary Information, Fig. S1). Additionally, the presence of elements of Pd, Zr, and Ce was verified by energy dispersive X-ray spectrometry. To observe the crystal structure of several CeO_2-ZrO_2-supported Pd catalysts, XRD measurements were performed. In contrast to ZrO_2, the structure of CeO_2-ZrO_2 was close to that of CeO_2 (see, Supplementary Information, Fig. S2) [48–52]. In addition, the diffraction peaks of Pd were not observed for the prepared catalysts including $Pd(NO_3)_2/CeO_2$-ZrO_2, $Pd(OH)_2/CeO_2$-ZrO_2, and PdO/CeO_2-ZrO_2, suggesting that these Pd species were highly dispersed on the supports (see, Supplementary Information, Fig. S3). When the 5 wt% PdO/CeO_2-ZrO_2 was reduced by pure H_2, the diffraction peak at 40° was assigned to the

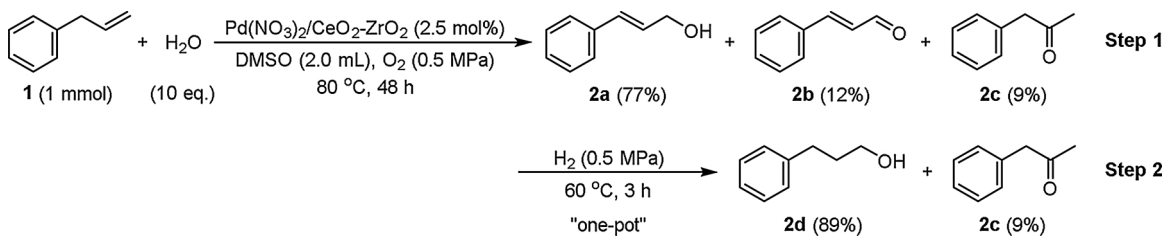

Scheme 2. Synthesis of 3-phenylpropan-1-ol from allylbenzene via a one-pot, two-step sequence.

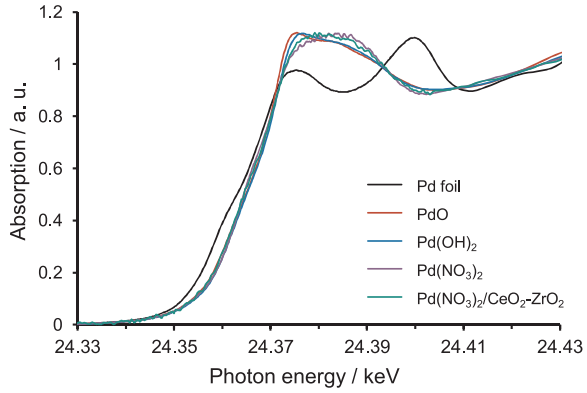

Fig. 1. Pd *K*-edge XANES spectra of Pd foil (black), PdO (red), $Pd(OH)_2$ (blue), $Pd(NO_3)_2$ (purple), $Pd(NO_3)_2/CeO_2$-ZrO_2 (green). (For interpretation of the references to colour in this figure legend, the reader is referred to the web version of this article).

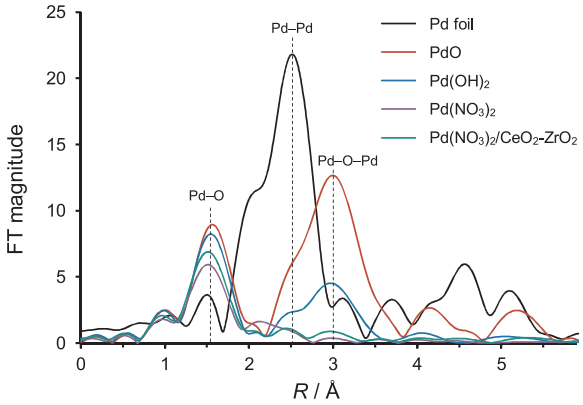

Fig. 3. Radial structure functions of Pd foil, PdO, $Pd(OH)_2$, $Pd(NO_3)_2$, and Pd $(NO_3)_2/CeO_2$-ZrO_2 (k = 3–11 $Å^{-1}$).

(111) plane of metallic Pd was confirmed (PDF-2 database, No. 00-001-1310) (Fig. S3d) [53].

To investigate the structure of the supported $Pd(NO_3)_2$, the catalyst was characterized by XAFS with the reference Pd foil, PdO, $Pd(OH)_2$, and $Pd(NO_3)_2$. The Pd *K*-edge X-ray absorption near edge structure (XANES) spectral feature of $Pd(NO_3)_2/CeO_2$-ZrO_2 resembled that of unsupported $Pd(NO_3)_2$ compared to those of PdO and $Pd(OH)_2$ in which the peak at 24.37 keV was more obvious (Fig. 1). A slight difference between $Pd(NO_3)_2/CeO_2$-ZrO_2 and unsupported $Pd(NO_3)_2$ might be due to the interaction of $Pd(NO_3)_2$ with the oxide support [54,55]. In addition, the k^3-weighted Pd *K*-edge extended X-ray absorption fine structure (EXAFS) oscillations patterns of $Pd(NO_3)_2/CeO_2$-ZrO_2 was also similar to that of unsupported $Pd(NO_3)_2$ and different from that of PdO and $Pd(OH)_2$ (Fig. 2).

In the radial structure functions (RSF) (Fig. 3), two peaks were mainly observed at about 1.53 Å and 3.0 Å in PdO and $Pd(OH)_2$. The peak in the range of 1.07–1.99 Å, which was attributed to Pd–O (first nearest-neighbor atoms) coordination, was observed in both $Pd(NO_3)_2/$

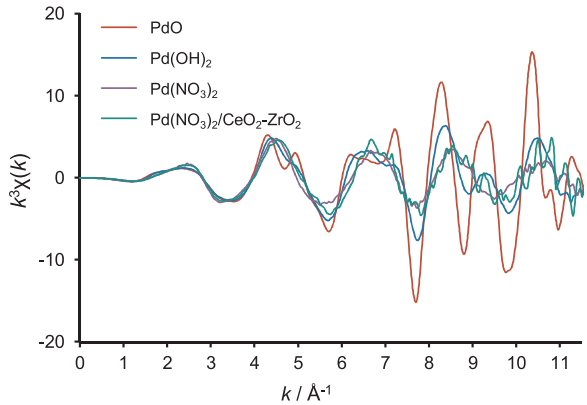

Fig. 2. k^3-weighted Pd *K*-edge EXAFS oscillations of PdO, $Pd(OH)_2$, $Pd(NO_3)_2$, and $Pd(NO_3)_2/CeO_2$-ZrO_2.

CeO_2-ZrO_2 and unsupported $Pd(NO_3)_2$. The structure parameters for Pd $(NO_3)_2/CeO_2$-ZrO_2 obtained by curve-fitting analysis using the structure model of $Pd(NO_3)_2$ (see, Supplementary Information, Tables S2 and S3). The coordination number for the first shell of $Pd(NO_3)_2/CeO_2$-ZrO_2 was 3.840 ± 1.013, which is close to the model $Pd(NO_3)_2$. The results supported the similarity of both materials. Moreover, the peak at about 3.0 Å (phase-uncorrected), which corresponded to the interaction of Pd—(O)—Pd for the second coordination shell [56–60], was not observed in neither $Pd(NO_3)_2/CeO_2$-ZrO_2 nor unsupported $Pd(NO_3)_2$. In addition, the peak at about 2.5 Å corresponding to the interaction of Pd—Pd was not observed in all these samples except Pd foil. Although the interaction between $Pd(NO_3)_2$ and the support could not be completely neglected, these spectral features indicated $Pd(NO_3)_2$ is probably deposited as it is on $Pd(NO_3)_2/CeO_2$-ZrO_2.

Moreover, the character of the deposited $Pd(NO_3)_2$ on CeO_2-ZrO_2 was studied by other chemisorption methods including CO_2-TPD and TPO. In the previous report, activation of the C—H bond of a terminal alkene was regarded as the rate-determining step in several Pd-catalyzed allylic C—H oxidation reactions, and the basicity of the catalytic system is crucial to promote the reaction [61]. In that regard, CO_2-TPD was employed to investigate the basicity of CeO_2-ZrO_2 and CeO_2-ZrO_2-supported Pd catalysts in Fig. 4. Firstly, the CO_2 desorption peak (m/z = 44) was observed for CeO_2-ZrO_2 at about 100 °C, revealed that the basic site was present on this support. These desorption peaks were observed on both $Pd(OH)_2/CeO_2$-ZrO_2 and $Pd(NO_3)_2/CeO_2$-ZrO_2, and a decrease in peak intensity on PdO/CeO_2-ZrO_2 might be caused by the calcination procedure. New peaks were observed on the catalysts in the range from 450 to 550 °C, suggesting that a new basic site was formed after the deposition of Pd species (Fig. 4b–d). Interestingly, another new desorption peak was observed by using $Pd(NO_3)_2$ as the precursor in the range from 220 to 280 °C for $Pd(OH)_2/CeO_2$-ZrO_2 and $Pd(NO_3)_2/CeO_2$-ZrO_2 with high intensity. It is reasonable that the basic sites were increased on the CeO_2-ZrO_2 supported $Pd(OH)_2$. However, according to the XAFS results, the structure of $Pd(NO_3)_2$ almost retained intact after the deposition onto the support. Therefore, the CO_2-TPD profile using m/z = 44 (CO_2 or N_2O) likewise have the possibility for desorption of the nitrate group. To this regard, the mass analysis for m/z = 30 (NO)

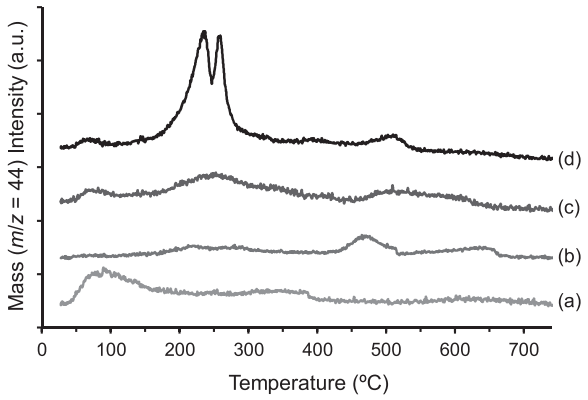

Fig. 4. CO_2-TPD profiles using m/z = 44 peak of (a) CeO_2-ZrO_2, (b) PdO/CeO_2-ZrO_2, (b) $Pd(OH)_2$/CeO_2-ZrO_2, and (d) $Pd(NO_3)_2$/CeO_2-ZrO_2.

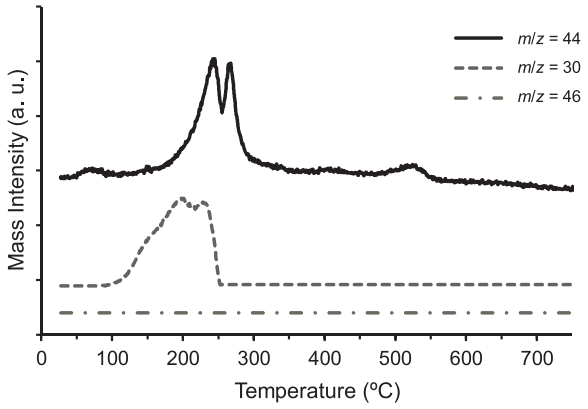

Fig. 5. CO_2-TPD profiles of $Pd(NO_3)_2$/CeO_2-ZrO_2.

and m/z = 46 (NO_2) was carried out. Despite the fact that the desorption peak of NO_2 was not observed (Fig. 5, Dash dot), the desorption peak of NO was detected from 120 to 250 °C (Fig. 5, Square dot), which is close to the peak for m/z = 44. As a consequence, the basic sites might be increased on 5 wt% $Pd(NO_3)_2$/CeO_2-ZrO_2, although the high intensity of the desorption peaks on $Pd(NO_3)_2$/CeO_2-ZrO_2 is still unclear. Besides, $Pd(NO_3)_2$/CeO_2-ZrO_2 was tested under TPO conditions mainly because O_2 is essential to promote the reactions as explained. The peak for m/z = 30 (NO) was observed in a wide range from 100 to 450 °C, and the peak for m/z = 44 (N_2O) was confirmed from 180 to 350 °C (see, Supplementary Information, Fig. S4). These results indicated that the decomposition of $Pd(NO_3)_2$ supported on CeO_2-ZrO_2 was occurred above 100 °C, furnishing the possibility for preserving the catalyst in a stable structure under the aerobic conditions.

To study the reaction pathway for the transformation of allylbenzene into cinnamyl alcohol, the effect of O_2, H_2O, and DMSO were investigated. First, a control experiment under the conditions of entry 13 in Table 1 was performed in the absence of O_2, and only trace amounts of products were obtained, revealing that O_2 is indispensable for promoting the reaction. Moreover, the recovered catalysts were analyzed by XRD (Fig. 6). A diffraction peak at 40° was observed for the catalyst recovered from the reaction mixture in the absence of O_2, indicating that the removal of nitrate groups and the aggregation of Pd species could cause a decrease in the catalytic activity. Thus, O_2 acts as a re-oxidizing agent for these Pd species. Since no product was observed under the conditions without H_2O, H_2O was confirmed as a reactant to assist the reaction. In addition, an isotope labeling experiment was carried out for entry 13 in Table 1 using water-^{18}O (97 atom% ^{18}O). As seen by GC–MS analysis, all the products contained more than 60 atom % ^{18}O after the reaction, suggesting that water-^{18}O served as a nucleophile to react with allylbenzene, and oxygen atom exchange

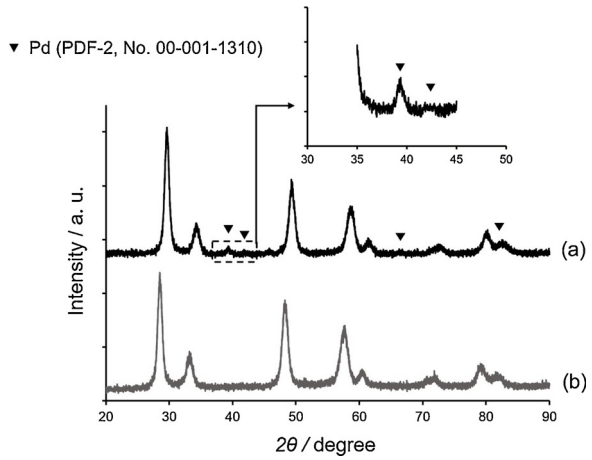

Fig. 6. Powder X-ray diffraction patterns of (a) the catalyst recovered from the reaction mixture in the absence of O_2 and (b) the catalyst recovered from the reaction mixture in the presence of O_2.

occurred between H_2O and O_2 (see, Supplementary Information, Scheme S2).

On the basis of the previous reports, the oxidative cleavage of an allylic C–H bond could be directly promoted by the Pd catalyst with strong Lewis acidity, such as $PdCl_2$ and $Pd(OAc)_2$. We anticipated that **1** was activated by supported $Pd(NO_3)_2$ to form a π-allyl Pd intermediate, followed by the addition of H_2O to the terminal position to give **2a** as the major product (Scheme 1). To slow down the aggregation of Pd, CeO_2-ZrO_2 was screened as a suitable support to maintain the $Pd(NO_3)_2$ species during the reaction. The basic surface of CeO_2-ZrO_2 might contribute to neutralize HNO_3 formed in the initial step. Also, the catalyst and intermediate were stabilized by using DMSO as the solvent [48], and O_2 acted as a vital role in the regeneration of Pd(II) species.

The recycling test of $Pd(NO_3)_2$/CeO_2-ZrO_2 for the transformation of allylbenzene into the primary alcohol was performed. Unfortunately, the catalytic activity was dramatically decreased in the second run for the reaction. In addition, the fresh and the spent catalysts were analyzed by XAFS (see, Supplementary Information, Figs. S5 and S6). The generation of Pd(0) was clearly observed in the spent catalyst [62]. Therefore, we consider that the deactivation of the catalyst was probably caused by the aggregation of $Pd(NO_3)_2$ into Pd(0) particles, although CeO_2-ZrO_2-supported $Pd(NO_3)_2$ exhibited better stability than the unsupported $Pd(NO_3)_2$, which was more easily aggregate to form Pd black precipitates during the reaction, resulting in much lower catalytic activity than $Pd(NO_3)_2$/CeO_2-ZrO_2.

3.3. Transformation of 1,3-butadiene into the corresponding primary alcohol

Next, we focused on the applicability of our catalysts to an industrial process. The transformation of 1,3-butadiene into butane-1,4-diol, which is widely used as a substrate for the production of various compounds with annual commercial scales of a million tons, has been particularly discussed [63]. In contrast to previous methods using acetylene and formaldehyde as the starting materials, 1,3-butadiene was regarded as the desired material for producing butane-1,4-diol. Mitsubishi Chemical has implemented a process to synthesize butane-1,4-diol from 1,3-butadiene. However, 1,3-butadiene has to undergo diacetoxylation to afford but-2-ene-1,4-diyl diacetate at the first stage, and three total steps are required, as described previously. To save energy and reduce the reaction steps, we attempted to explore a new approach in which 1,3-butadiene directly reacts with H_2O to build 2-butene-1,4-diol and then provide butane-1,4-diol by a simple hydrogenation in a “one-pot” manner. At first, the reactions were performed in an autoclave, and the results are summarized in Table 2.

Table 2
Reaction conditions for the transformation of 1,3-butadiene.[a]

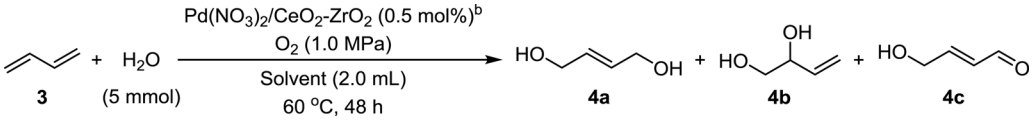

Entry	Catalyst[b]	Amount of **3** (eq.)[b,c]	Solvent	Yield (%)[d]			TONs[b]
				4a	**4b**	**4c**	
1	5 wt% $Pd(NO_3)_2/CeO_2$-ZrO_2	9	DMSO	31	29	24	168
2	5 wt% $Pd(NO_3)_2/CeO_2$-ZrO_2	6	EtOAc	18	14	16	96
3	5 wt% $Pd(NO_3)_2/CeO_2$-ZrO_2	12	EtOAc	16	13	15	88
4	5 wt% $Pd(NO_3)_2/CeO_2$-ZrO_2	5	1,4-dioxane	26	21	18	130
5	5 wt% $Pd(NO_3)_2/CeO_2$-ZrO_2	6	MeOH	35	19	20	148
6[e]	5 wt% $Pd(NO_3)_2/CeO_2$-ZrO_2	7	MeOH	33	33	23	178
7	5 wt% $Pd(OH)_2/CeO_2$	10	DMSO	31	27	21	158
8	5 wt% Pd/CeO_2	8	EtOAc	20	29	32	162

[a] Reaction conditions: H_2O (5 mmol), **3** (5–12 eq.), supported Pd catalyst (Pd 0.5 mol%), Solvent (2 mL), O_2 (1.0 MPa), 60 °C, 48 h.
[b] Calculated based on H_2O.
[c] Amount of 1,3-butadiene was estimated though subtraction of the bottle before and after addition.
[d] GC analysis based on H_2O with tridecane as an internal standard.
[e] Reacted at 70 °C for 36 h.

Table 3
Transformation of 1,3-butadiene by a continuous gas flow reactor.[a]

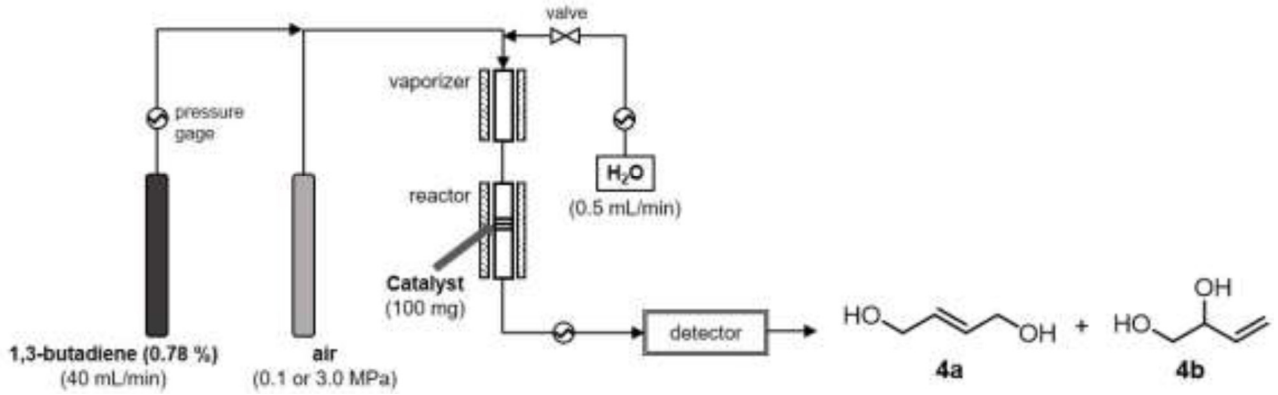

Entry	Catalyst[b]	Air (MPa)	Temp. (°C)	Time (h)	Space-time yield (mmol/kg-cat · h)[c]	
					4a	**4b**
1	Pd/ZrO_2	3.0	80	0–2	116	99
				2–4	153	87
				4–6	n. d.	n. d.
2	$Pd(OH)_2/CeO_2$-ZrO_2	3.0	80	0–2	127	24
				2–4	61	n. d.
				4–6	47	n. d.
3	$Pd(NO_3)_2/CeO_2$-ZrO_2	3.0	80	0–2	766	128
				2–4	155	n. d.
				4–6	240	26
4	$Pd(NO_3)_2/CeO_2$-ZrO_2	0.1	80	0–2	21	n. d.
				2–4	113	n. d.
				4–6	131	n. d.
5	$Pd(NO_3)_2/CeO_2$-ZrO_2[d]	3.0	60	0–2	267	149
				2–4	134	108
				4–6	139	76

[a] Reaction conditions: 1,3-butadiene, catalyst (100 mg), H_2O (0.5 mL/min), air (0.1 or 3.0 MPa), vaporizer temperature (130 °C), reactor temperature (60 or 80 °C), 0–6 h.
[b] The catalysts were prepared with a Pd loading of 5 wt%.
[c] Analyzed by GC based on 1,3-butadiene using diglyme as an internal standard.
[d] 10 wt% $Pd(NO_3)_2/CeO_2$-ZrO_2 was used.

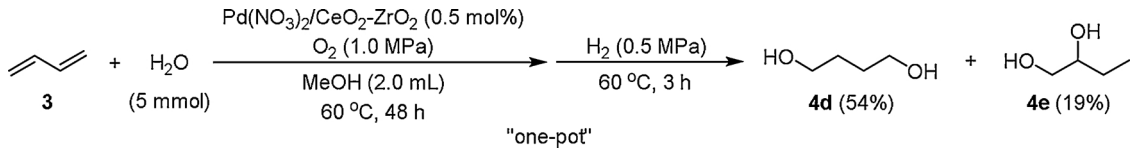

Scheme 3. Synthesis of butane-1,4-diol from 1,3-butadiene via a one-pot, two-step sequence.

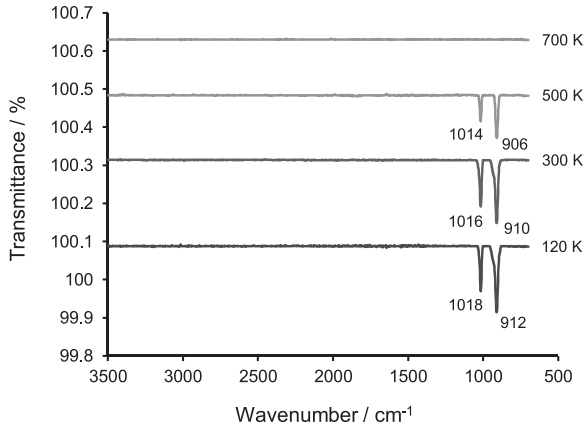

Fig. 7. IRAS measurements for the adsorption of 1,3-butadiene on the Pd(111) surface from -153.15 °C (120 K) to 426.85 °C (700 K).

According to the analysis of the reaction mixture, *trans*-2-butene-1,4-diol (**4a**), 3-butene-1,2-diol (**4b**), and *trans*-4-hydroxybut-2-enal (**4c**) were detected as the main products. The *cis* isomers of the products and other ketone byproducts such as methyl vinyl ketone were not observed in this process. Additionally, telomerization byproducts, such as 2,7-octadien-1-ol, were not formed over the supported Pd catalysts. The amount of 1,3-butadiene was measured by weighing. The GC yields and TONs were calculated based on the amount of H_2O added. Using CeO_2-ZrO_2-supported $Pd(NO_3)_2$ as the catalyst and DMSO as the solvent, **4a** could be obtained in more than 30% yield, but the yields of **4b** and **4c** were also high (Table 2, entry 1). When ethyl acetate (EtOAc) and 1,4-dioxane were used, the yield and selectivity of **4a** were not satisfactory (Table 2, entries 2 and 4). The reaction proceeded well in MeOH to allow the production of **4a** with relatively high selectivity, accordingly, the TON was calculated to be 148 (Table 2, entry 5). The contrast experiment results showed that the lower reaction temperature tends to improve the selectivity of primary alcohol, although the TON reached 178 in entry 6 (Table 2, entry 5 vs. entry 6). Therefore, the reaction conditions in entry 5 were chosen as the optimized conditions to synthesize butane-1,4-diol. As described in Scheme 3, compounds **4a** and **4c** could be reduced by H_2 to give butane-1,4-diol (**4d**) in 54% yield, and butane-1,2-diol (**4e**) was observed as the byproduct. Although Kuznetsova et al. reported a similar process for the transformation of **3** over PdTe/C, the reactions were performed at 90–100 °C to give **4a** in moderate yields [28]. Therefore, $Pd(NO_3)_2$/CeO_2-ZrO_2 not only provided a mild and efficient synthetic method for the synthesis of **4a** but also realized the direct production of **4d** from **3** through a "one-pot" process for the first time. In addition, the reactivities of 1,3-butadiene and allylbenzene over a supported Pd catalyst was disunity, because $Pd(OH)_2$/CeO_2 and even Pd/CeO_2 enabled the efficient transformation of 1,3-butadiene into **4a** (Table 2, entries 7 and 8), suggesting that control of the product selectivity will be the considerable subject for each substrate.

Furthermore, a continuous gas flow reactor was developed to promote the direct reaction between 1,3-butadiene and H_2O. First, 1,3-butadiene was refrigerated at 0 °C to obtained its liquefied form, then injected with H_2O into a vaporizer and introduced into a reactor containing 100 mg $Pd(NO_3)_2$/CeO_2-ZrO_2 (see, Supplementary Information, Fig. S7). The reaction was performed at 80 °C for 4 h, affording **4a** and **4b** as the major products. However, during the reaction, the polymerization of 1,3-butadiene was difficult to avoid, although an inhibitor, such as hydroquinone or 4-*tert*-butylcatechol, was employed. Consequently, we replaced pure 1,3-butadiene with a mixed gas containing 0.78% 1,3-butadiene in N_2 for optimizing the reaction conditions in our gas flow reactor (Table 3). Pressurized air was used instead of O_2 due to safety concerns for industrial production. In this reaction, the mixed 1,3-butadiene gas directly reacted with H_2O in the presence of the catalyst, and the reaction mixture was analyzed every 2 h to evaluate the catalytic activity by calculating the space-time yield (STY). By comparison with Pd/ZrO_2 and $Pd(OH)_2$/CeO_2-ZrO_2, $Pd(NO_3)_2$/CeO_2-ZrO_2 was deemed suitable for primary alcohol synthesis (Table 3, entries 1–3). Unlike the batch reactor, product **4c** was not detected in the gas flow reactor; additionally, a much better selectivity of **4a** was confirmed, and the STY reached 766 mmol/kg-cat · h for the initial 2 h at 80 °C (Table 3, entry 2). We also tested the reaction under 0.1 MPa air or at 60 °C. The yields were dramatically decreased for all products (Table 3, entries 4 and 5). The relatively low temperature and good selectivity provide a promising alternative for the production of butane-1,4-diol with sophisticated instruments.

In this study, it is interesting that the telomerization of 1,3-butadiene was completely inhibited in the reactions catalyzed by these supported Pd species, while the telomerization byproduct is generated in a notable quantity from a bis-π-allyl Pd intermediate when homogeneous catalysts are used [31]. However, as mentioned above, only *trans*-2-butene-1,4-diol was observed during the product analyses. We considered that the specific adsorption structure of 1,3-butadiene on the catalyst probably led to these features. Since supported Pd(0) catalyst also promoted the transformation of 1,3-butadiene to form **4a** and **4b** (Table 2, entry 8 and Table 3, entry 1) as well as supported Pd(II) catalyzed reactions, the adsorption structure of 1,3-butadiene on the Pd single-crystal surface was subsequently investigated by infrared reflection absorption spectroscopy (IRAS) on the clean Pd(111) surface. Fig. 7 shows an IRAS for the Pd(111) surface exposed to 1,3-butadiene of 15 L (1 L = 1×10^{-6} Torr/s) from approximately -153.15 (120 K) to 426.85 °C (700 K). At -153.15 °C, peaks due to out-of-plane bending vibrations of ω(CH_2) and τ(CH_2) were observed at 912 and 1018 cm^{-1}, respectively. Accordingly, these peaks were confirmed at 26.85 (300 K) and 226.85 °C (500 K), and the intensities decreased with increasing temperature. These results suggested that the adsorption structure of 1,3-butadiene on the Pd(111) surface was almost identical over a wide temperature range. In addition, 1,3-butadiene was desorbed when the temperature arrived at 426.85 °C (700 K). On the other hand, peaks for the stretching vibrations of C—C, C=C, CH, and CH_2 were observed in addition to peaks of ω(CH_2) and τ(CH_2) in the high-resolution electron energy loss spectrum of 1,3-butadiene adsorbed on the Pd(110) surface [64]. In IRAS, the vibration mode parallel to the surface was not detected due to the surface selection rule. Therefore, no peaks corresponding to stretching vibrations of C—C, C=C, CH, or CH_2 were observed in the IRAS (Fig. 7), indicating that the molecular plane of 1,3-butadiene adsorbed on the Pd(111) surface was parallel to the surface. Moreover, the wavenumbers of ω(CH_2) and τ(CH_2) observed in this study are close to those reported for 1,3-butadiene adsorbed in the *s-trans* form on Au(111) (ω(CH_2): 916 cm^{-1}, τ(CH_2): 1007 cm^{-1}) [65], suggesting that 1,3-butadiene adsorbed on Pd(111) has an adsorption structure in the *s-trans* form.

In addition, we investigated the adsorption of 1,3-butadiene on Pd(111) pre-adsorbed with oxygen (θ_O = 0.25), which was produced by

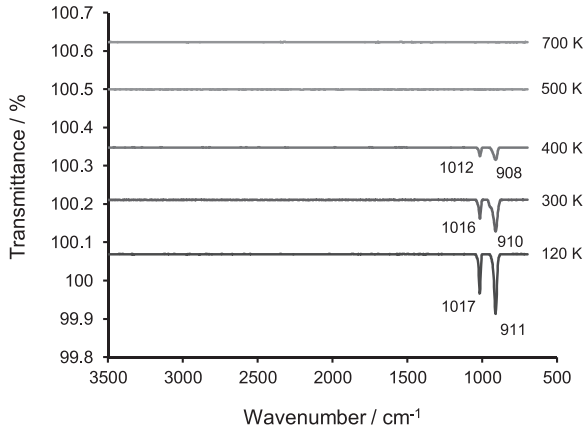

Fig. 8. IRAS measurements for the adsorption of 1,3-butadiene on Pd(111) pre-adsorbed with oxygen ($\theta_O = 0.25$) from -153.15 °C (120 K) to 426.85 °C (700 K).

exposing O_2 to 100 L in the same temperature range. A θ value of 1 corresponds to a Pd(111) surface atom density of 1.53×10^{15} atoms/cm^2. IRAS measurements were performed for the O/Pd(111) surface exposed to 1,3-butadiene under the same conditions as the clean Pd (111) surface. As a result, absorption peaks of $\omega(CH_2)$ (911 cm^{-1}) and $\tau(CH_2)$ (1017 cm^{-1}) were observed at −153.15 °C, and these peaks could be detected until the temperature reached 226.85 °C (Fig. 8). The wavenumbers of these peaks are in good agreement with those observed for a clean Pd(111) surface (Fig. 7), demonstrating that co-adsorbed oxygen had no influence on the adsorption structure of 1,3-butadiene on the Pd surface. That is, the electronic states of surface Pd are cationic, but there is no change in the adsorption states of 1,3-butadiene.

Next, the thermal reactivities of 1,3-butadiene adsorbed on clean Pd(111) and O/Pd(111) surfaces were examined by X-ray photoelectron spectroscopy (XPS). At -153.15 °C, the C1s peak was observed at 285.1 eV on both surfaces, which was attributed to the carbon of 1,3-butadiene [66]. When both surfaces were heated from -153.15 °C to 26.85 °C at a heating rate of 20 °C/min, the peak area decreased, but the peak position was maintained, indicating that some of the adsorbed 1,3-butadiene desorbed. On the clean Pd(111) surface, when the temperature was increased to 226.85 °C (500 K), the peak shifted to lower binding energy (Fig. 9). This indicates that the decomposition of 1,3-butadiene occurred. At approximately 426.85 °C, a peak was observed at 284.6 eV, due to the atomic carbon formed by the dehydrogenation of 1,3-butadiene. When the temperature was further increased to 726.85 °C (1000 K), the peak disappeared, as the atomic carbon migrated into the Pd bulk. On the other hand, a peak for atomic carbon

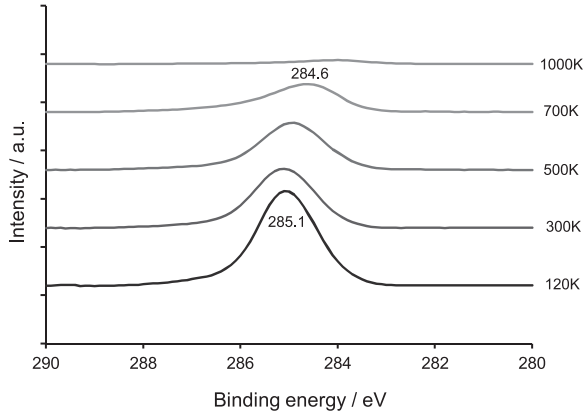

Fig. 9. XPS C1s analysis for 1,3-butadiene on Pd(111) under programmed temperature conditions from -153.15 °C (120 K) to 726.85 °C (1000 K).

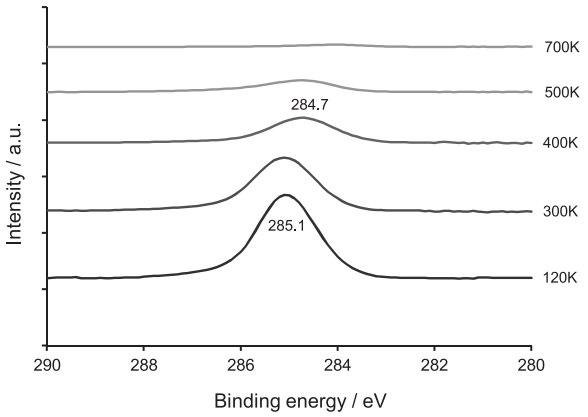

Fig. 10. XPS C1s analysis for 1,3-butadiene on Pd(111) pre-adsorbed with oxygen ($\theta_O = 0.25$) under programmed temperature conditions from -153.15 °C (120 K) to 426.85 °C (700 K).

(~284.7 eV) was observed at 126.85 °C (400 K) on the O/Pd(111) surface (Fig. 10). That is, atomic carbon was formed on the O/Pd(111) surface at a lower temperature than on the clean Pd(111) surface. We confirmed that pre-adsorbed oxygen remains on this surface. Therefore, we consider that the formation of atomic carbon by the dehydrogenation of 1,3-butadiene was promoted due to the change in the electronic states of surface Pd atoms by the adsorbed oxygen.

The reaction pathway for the transformation of 1,3-butadiene with H_2O was speculated (Fig. 11). According to the results of the product analyses and surface experiments, 1,3-butadiene might be adsorbed on the supported Pd catalyst in the *s-trans* form, and one H_2O molecule was initially added to the terminal position to afford a π-allyl Pd intermediate. Then, the π-allyl Pd intermediate on the metal oxide was attacked by another H_2O molecule to give **2b** as a major product, and **2c** was formed as a minor product due to the steric effect. The adsorption structure of the *s-cis* form was not observed in our surface experiments, and the corresponding products were not detected either. The formation of the telomerization product was successfully inhibited over the supported Pd catalysts.

4. Conclusion

In conclusion, an atom-efficient approach for the direct synthesis of primary alcohols from terminal alkenes and H_2O is established in this work. Using environmentally benign O_2 and H_2 as the sole oxidant and reductant, respectively, resulted in the formation of H_2O as the only theoretical byproduct. Achievement of the products with high *anti*-Markovnikov selectivity successfully shorten the steps in comparison to conventional synthesis route. CeO_2-ZrO_2-supported $Pd(NO_3)_2$ was found to be an efficient catalyst for transform allylbenzene into cinnamyl alcohol. The final product, 3-phenylpropan-1-ol, could be obtained from a one-pot sequence in good yield. The analyses of the catalyst revealed that the highly dispersed molecular $Pd(NO_3)_2$ on CeO_2-ZrO_2 possibly acted significant role to promote this reaction. Unfortunately, the catalytic activity was significantly decreased in the recycling test caused by the formation of Pd(0) particles during the reaction.

In addition, the catalyst allowed the production of *trans*-butane-1,4-diol from 1,3-butadiene in a batch reactor. The adsorption structure of 1,3-butadiene on Pd(111) was confirmed as *s-trans* by IRAS observations. Finally, a continuous gas flow reactor was successfully developed to achieve good *anti*-Markovnikov selectivity for the transformation of 1,3-butadiene into *trans*-2-butene-1,4-diol. These reactions were generally carried out under relatively mild conditions, and thus possess the remarkable potential for industrial applications. Further studies on the reaction mechanism and general feasibility of substrates are in progress.

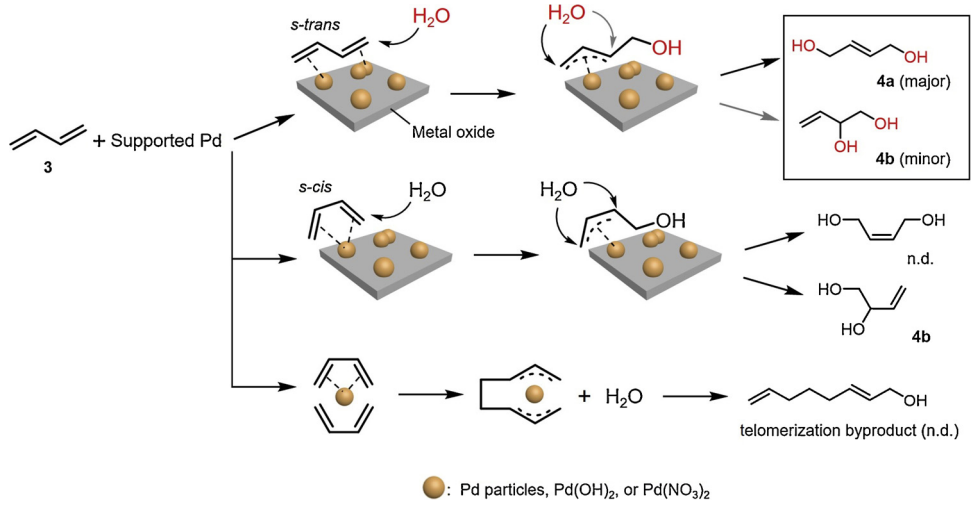

Fig. 11. Speculated reaction pathway for the transformation of 1,3-butadiene with H_2O on a supported Pd catalyst.

Acknowledgements

This work was financially supported by the ALCA program (No: 11102798) from the Japan Science and Technology Agency and Mitsubishi Chemical Corporation.

The synchrotron radiation experiments were performed at the BL14B2 of SPring-8 with the approval of the Japan Synchrotron Radiation Institute (JASRI), proposal Nos. 2014B1897, 2016A1521, and 2017A1780.

HAADF-STEM observations were performed at the Ultramicroscopy Research Center, Kyushu University.

Appendix A. Supplementary data

Supplementary material related to this article can be found, in the online version, at doi:https://doi.org/10.1016/j.apcatb.2019.01.031.

References

[1] B. Trost, Science 254 (1991) 1471–1477.
[2] B. Trost, Angew. Chem. Int. Ed. 34 (1995) 259–281.
[3] R. Sheldon, Pure Appl. Chem. 72 (2000) 1233–1246.
[4] S. Biswas, A. Poyraz, Y. Meng, C. Kuo, C. Guild, H. Tripp, S. Suib, Appl. Catal. B: Environ. 165 (2015) 731–741.
[5] Q. Wang, X. Cai, Y. Liu, J. Xie, Y. Zhou, J. Wang, Appl. Catal. B: Environ. 189 (2016) 242–251.
[6] J. Zhu, J. Wood, K. Deplanche, I. Mikheenko, L. Macaskie, Appl. Catal. B: Environ. 199 (2016) 108–122.
[7] C. Weerakkody, S. Biswas, W. Song, J. He, N. Wasalathanthri, S. Dissanayake, D. Kriz, B. Dutta, S. Suib, Appl. Catal. B: Environ. 221 (2018) 681–690.
[8] M. Sun, J. Xia, H. Wang, X. Liu, Q. Xia, Y. Wang, Appl. Catal. B: Environ. 227 (2018) 488–498.
[9] J. Song, Z. Huang, L. Pan, K. Li, X. Zhang, L. Wang, J. Zou, Appl. Catal. B: Environ. 227 (2018) 386–408.
[10] H.A. Wittcoff, B.G. Reuben, J.S. Plotkin, Industrial Organic Chemistry, 2nd ed., John Wiley & Sons: New Jersey, 2004.
[11] J. Falbe, H. Bahrmann, W. Lipps, D. Mayer, Ullmann's Encyclopedia of Industrial Chemistry, Electronic Release, 7th ed., Wiley-VCH, Weinheim, 2009.
[12] J. Haggin, Chem. Eng. News 71 (1993) 23–27.
[13] T. Mitsudome, T. Umetani, N. Nosaka, K. Mori, T. Mizugaki, K. Ebitani, K. Kaneda, Angew. Chem. Int. Ed. 45 (2006) 481–485.
[14] M.B. Smith, J. March, March's Advanced Organic Chemistry, John Wiley & Sons, New Jersey, 2001.
[15] K. Takahashi, M. Yamashita, T. Ichihara, K. Nakano, K. Nozaki, Angew. Chem. Int. Ed. 49 (2010) 4488–4490.
[16] G. Dong, P. Teo, Z.K. Wickens, R.H. Grubbs, Science 16 (2011) 1609–1612.
[17] J. Tsuji, Synthesis (1990) 739–749.
[18] Mitsubishi Kasei Corporation, ChemTech, 1988, p. 759.
[19] R. Ashford, Ashford's Dictionary of Industrial Chemicals, 3rd ed., (2011) Wavelength, London.
[20] X. Zhou, L. Ren, P. Wang, J. Org. Chem. 82 (2017) 9794–9800.
[21] Y. Li, L. Li, M. Yang, G. He, E. Kantchev, J. Org. Chem. 82 (2017) 4907–4917.
[22] S. Vemula, D. Kumar, G. Cook, ACS Catal. 6 (2016) 5295–5301.
[23] C. Li, M. Li, J. Li, J. Liao, W. Wu, H. Jiang, J. Org. Chem. 82 (2017) 10912–10919.
[24] W. Yang, H. Chen, J. Li, C. Li, W. Wu, H. Jiang, Chem. Commun. 51 (2015) 9575–9578.
[25] K. Michigami, T. Mita, Y. Sato, J. Am. Chem. Soc. 139 (2017) 6094–6097.
[26] X. Qi, P. Chen, G. Liu, Angew. Chem. Int. Ed. 56 (2017) 9517–9521.
[27] C. Li, H. Chen, J. Li, M. Li, J. Liao, W. Wu, H. Jiang, Adv. Synth. Catal. 360 (2018) 1600–1604.
[28] N. Kuznetsova, V. Zudin, L. Kuznetsova, V. Zaikovskii, H. Kajitani, M. Utsunomiya, K. Takahashi, Appl. Catal. A Gen. 513 (2016) 30–38.
[29] T. Mitsudome, T. Umetani, N. Nosaka, K. Mori, T. Mizugaki, K. Ebitani, K. Kaneda, Angew Chem. Int. Ed. 45 (2006) 481–485.
[30] A.N. Campbell, P.B. White, L.A. Guzei, S.S. Stahl, J. Am. Chem. Soc. 132 (2010) 15116–15119.
[31] K.E. Atkins, W.E. Walker, R.M. Manyik, J. Chem. Soc. D. (1971) 330–330.
[32] R. Tomita, K. Mantani, A. Hamasaki, T. Ishida, M. Tokunaga, Chem. Eur. J. 20 (2014) 9914–9917.
[33] X. Liu, B. Hu, K. Fujimoto, M. Haruta, M. Tokunaga, Appl. Catal. B: Environ. 92 (2009) 411–421.
[34] T. Ishida, H. Watanabe, T. Takei, A. Hamasaki, M. Tokunaga, M. Haruta, Appl. Catal. A: General. 425 (426) (2012) 85–90.
[35] A. Hamasaki, Y. Yasutake, T. Norio, T. Ishida, T. Akita, H. Ohashi, T. Yokoyama, T. Honma, M. Tokunaga, Appl. Catal. A: Gen. 469 (2014) 146–152.
[36] J. Cai, F. Jiang, X. Liu, Appl. Catal. B: Environ. 210 (2017) 1–13.
[37] B. Gu, V. Ordomsky, M. Bahri, O. Ersen, P. Chernavskii, D. Filimonov, A. Khodakov, Appl. Catal. B: Environ. 234 (2018) 153–166.
[38] T. Ishida, R. Tsunoda, Z. Zhang, A. Hamasaki, T. Honma, H. Ohashi, T. Yokoyama, M. Tokunaga, Appl. Catal. B: Environ. 150 (151) (2014) 523–531.
[39] T. Ishida, Z. Zhang, H. Murayama, M. Tokunaga, J. Synth. Org. Chem., Jpn. 75 (2017) 1150–1161.
[40] Z. Zhang, Q. Wu, T. Hashiguchi, T. Ishida, H. Murayama, M. Tokunaga, Catal. Commun. 87 (2016) 18–22.
[41] Z. Zhang, Y. Kumamoto, T. Hashiguchi, T. Mamba, H. Murayama, E. Yamamoto, T. Ishida, T. Honma, M. Tokunaga, ChemSusChem 10 (2017) 3482–3489.
[42] S. Soomro, F. Ansari, K. Chatziapostolou, K. Kohler, J. Catal. 273 (2010) 138–146.
[43] T. Honma, H. Oji, S. Hirayama, Y. Taniguchi, H. Ofuchi, M. Takagaki, AIP Conf. Proc. 1234 (2010) 13–16.
[44] H. Oji, Y. Taniguchi, S. Hirayama, H. Ofuchi, M. Takagaki, T. Honma, J. Synchrotron Radiat. 19 (2012) 54–59.
[45] B. Ravel, M. Newville, J. Synchrotron Radiat. 12 (2005) 537–541.
[46] T. Diao, D. Pun, S. Stahl, J. Am. Chem. Soc. 135 (2013) 8205–8212.
[47] Z. Zhang, T. Hashiguchi, T. Ishida, A. Hamasaki, T. Honma, H. Ohashi, T. Yokoyama, M. Tokunaga, Org. Chem. Front. 2 (2015) 654–660.
[48] C. Orge, J. Órfão, M. Pereira, A. Duarte de Farias, R. Rabelo Neto, M. Fraga, Appl. Catal. B: Environ. 103 (2011) 190–199.
[49] G. Pantaleo, V. Parola, F. Deganello, R. Singha, R. Bal, A. Venezia, Appl. Catal. B: Environ. 189 (2016) 233–241.
[50] H. Zhang, C. Wu, W. Wang, J. Bu, F. Zhou, B. Zhang, Q. Zhang, Appl. Catal. B: Environ. 227 (2018) 209–217.
[51] W. Yang, C. Li, H. Wang, X. Li, W. Zhang, H. Li, Appl. Catal. B: Environ. 239 (2018) 233–244.
[52] B. Wang, B. Chen, Y. Sun, H. Xiao, X. Xu, M. Fu, J. Xu, L. Chen, D. Ye, Appl. Catal. B: Environ. 238 (2018) 328–338.
[53] J. Gu, C. Hu, W. Zhang, A. Dichiara, Appl. Catal. B: Environ. 237 (2018) 482–490.
[54] M. Benkhaled, S. Morin, C. Pichon, C. Thomazeau, C. Verdon, D. Uzio, Appl. Catal. A: Gen. 312 (2006) 1–11.
[55] E. Dann, E. Gibson, R. Catlow, P. Collier, T. Erden, D. Gianolio, C. Hardacre, A. Kroner, A. Raj, A. Goguet, P. Wells, Chem. Mater. 29 (2017) 7515–7523.
[56] H. Yoshida, T. Nakajima, Y. Yazawa, T. Hattori, Appl. Catal. B: Environ. 71 (2007) 70–79.

[57] R. Yoshimoto, T. Ninomiya, K. Okumura, M. Niwa, Appl. Catal. B: Environ. 75 (2007) 175–181.
[58] X. Guo, M. Meng, F. Dai, Q. Li, Z. Zhang, Z. Jiang, S. Zhang, Y. Huang, Appl. Catal. B: Environ. 142 (143) (2013) 278–289.
[59] M. Ren, Y. Kang, W. He, Z. Zou, X. Xue, D.L. Akins, H. Yang, S. Feng, Appl. Catal. B: Environ. 104 (2007) 49–53.
[60] Y. Liu, Y. Zhou, J. Li, Q. Wang, Q. Qin, W. Zhang, H. Asakura, N. Yan, J. Wang, Appl. Catal. B: Environ. 209 (2017) 679–688.
[61] C. Engelin, T. Jensen, S. Rodriguez-Rodriguez, P. Fristrup, ACS Catal. 3 (2013) 294–302.
[62] G. Celik, S. Ailawar, S. Gunduz, J. Miller, P. Edmiston, U. Ozkan, Appl. Catal. B: Environ. 239 (2018) 654–664.
[63] R. Satta, N. Dimitrijevic, H. Manev, Eur. J. Pharmacol. 473 (2003) 149–152.
[64] S. Katano, S. Ichihara, H. Ogasawara, H. Kato, T. Komeda, M. Kawai, K. Domen, Surf. Sci. 502 (503) (2002) 164–168.
[65] N. Osaka, M. Akita, K. Itoh, J. Phys. Chem. B 102 (1998) 6817–6824.
[66] J. Silvestre-Albero, M. Borasio, G. Rupprechter, H. Freund, Catal. Commun. 8 (2007) 292–298.